Formation and mechanical properties of Cu–Hf–Ti bulk glassy alloys

Akihisa Inoue
Institute for Materials Research, Tohoku University, Sendai 980-8577, Japan and Inoue Superliquid Glass Project, Exploratory Research for Advanced Technology, Japan Science and Technology Corporation, Sendai 982-0807, Japan

Wei Zhang
Inoue Superliquid Glass Project, Exploratory Research for Advanced Technology, Japan Science and Technology Corporation, Sendai 982-0807, Japan

Tao Zhang
Institute for Materials Research, Tohoku University, Sendai 980-8577, Japan

Kei Kurosaka
Graduate School, Tohoku University, Sendai 980-8577, Japan

(Received 15 May 2001; accepted 19 July 2001)

High-strength Cu-based bulk glassy alloys were formed in the Cu–Hf–Ti system by the copper mold casting and melt clamp forging methods. The maximum diameter is 4 mm for the $Cu_{60}Hf_{25}Ti_{15}$ alloy. The substitution of Hf in the $Cu_{60}Hf_{40}$ alloy by Ti causes an increase in the glass-forming ability (GFA). As the Ti content increases, the glass transition temperature (T_g) decreases, while the crystallization temperature (T_x) shows a maximum at 5% Ti and then decreases, resulting in a maximum supercooled liquid region ΔT_x ($= T_x - T_g$) of 78 K at 5% Ti. The liquidus temperature (T_l) has a minimum of 1172 K around 20% Ti, and hence, a maximum T_g/T_l of 0.62 is obtained at 20% Ti. The high GFA was obtained at the compositions with high T_g/T_l. The bulk glassy alloy exhibits tensile fracture strength of 2130 MPa, compressive fracture strength of 2160 MPa, and compressive plastic elongation of 0.8 to 1.6%. The new Cu-based bulk glassy alloys with high T_g/T_l above 0.60, high fracture strength above 2100 MPa, and distinct plastic elongation are encouraging for future development as a new type of bulk glassy alloy that can be used for structural materials.

I. INTRODUCTION

Since the findings of glassy alloys with a large supercooled liquid region before crystallization in Ln–Al–TM[1] and Mg–Ln–TM[2] (Ln = lanthanide metals) systems, followed by the formations of Ln-[3] and Mg-based[4] bulk glassy alloys by use of the high stability of supercooled liquid against crystallization, a number of bulk glassy alloys have been developed in multicomponent systems such as Zr,[5,6] Ti,[7] Fe,[8] Pd–Cu,[9] Ni,[10] and Co[11] bases. Thus, the bulk glassy alloys have been extended to engineering important alloy systems including Fe-, Co-, Ni-, Ti-, and Mg-based alloys. However, there have been no data on the formation of bulk glassy alloys in Al- and Cu-based alloy systems containing more than 50 at.% Al or Cu, though their formations are expected to cause significant extension of application fields of bulk glassy alloys. It is well known that amorphous alloys in a thin ribbon form are formed in a number of Al-[12,13] and Cu-based[14] systems by the melt-spinning technique. The previous data have also reported that the choice of Al–Y–Co–Ni[15] and Cu–Ti–Zr[16] systems leads to the formation of amorphous alloys with thickness of about 0.8 and 1 mm, respectively. Recently, intensive developments of Cu-based bulk glassy alloys were made by the increase of Cu content and the decrease in Al content in the Zr–Al–Ni–Cu[5] and Zr–Ti–Al–Ni–Cu[17] base systems and some bulk glassy alloys containing Cu contents up to 40 at.% Cu have been obtained in Cu–Ti–Zr–Ni,[18] Cu–Ti–Ni–Si–B,[19] and Cu–Ti–Zr–Ni–Sn[20] systems. Very recently, we have reported that Cu-based bulk glassy alloys with a thickness of 4 mm are formed in the Cu–Zr–Ti ternary system and the bulk glassy alloys exhibit good mechanical properties.[21] As is the case for the developmental history for a number of bulk glassy alloys developed to date,[22–24] the first success of forming bulk glassy alloys in the Cu-based ternary system defined by Cu contents more than 50 at.% allows us to expect the subsequent synthesis of bulk glassy alloys in different Cu-based systems. Considering the similarities of atomic radius and atomic electronic negativity between Zr and

Hf elements belonging to the same group number in the periodic table,[25] similar bulk glassy alloys are also expected to be formed in the Cu–Hf–Ti system. This paper presents the composition range in which a glassy phase is formed in the Cu–Hf–Ti system by copper mold casting and the compositional dependence of thermal stability and mechanical properties of the bulk glassy alloys. The reason for the high glass-forming ability in the ternary system is also discussed.

II. EXPERIMENTAL PROCEDURE

Ternary Cu–Hf–Ti alloys were prepared by arc melting the mixtures of pure Cu, Hf, and Ti metals in an argon atmosphere. Ribbon samples with a cross section of 0.02×1.2 mm^2 were prepared by melt spinning. Bulk alloys in a cylindrical form with a length of 60 mm and diameters up to 5 mm were prepared by copper mold casting. In addition, bulk alloys in a sheet form with a dimension of $50 \times 100 \times 2$ mm^3 were also prepared by the melt clamp forging technique.[26,27] Glassy structure was identified by x-ray diffraction (XRD), transmission electron microscopy, and optical microscopy. Thermal stability associated with glass transition temperature (T_g) and crystallization temperature (T_x) was examined by differential scanning calorimetry (DSC) at a heating rate of 0.67 K/s. The melting temperature was determined by differential thermal analysis (DTA) at a heating rate of 0.17 K/s. Mechanical properties were measured with an Instron-type testing machine. The gauge dimensions were 1 mm in thickness, 2 mm in width, and 10 mm in length for tensile tests and 2 mm in diameter and 4 mm in height for compressive tests. Fracture surface was examined by scanning electron microscopy. Hardness was measured with a Vickers hardness indenter under a load of 1 kg.

III. RESULTS

A. Thermal stability of supercooled liquid

It has previously been reported that a glassy phase in the Cu–Hf binary system is formed in a wide composition range of 30 to 70 at.% Hf.[28] Figure 1 shows DSC curves of the melt-spun Cu_{100-x} Hf_x (x = 30 to 70 at.%) glassy alloys. Although no glass transition is observed for the 30% Hf and 70% Hf alloys, the alloys containing 40% to 60% Hf exhibit the distinct glass transition, followed by a large supercooled liquid region before crystallization. The T_g and T_x decrease with increasing Hf content from 40% to 60%, despite that the liquidus temperature of Hf metal is much higher than that of Cu metal. It is also seen that the supercooled liquid region defined by the temperature interval between T_g and T_x, ΔT_x ($= T_x - T_g$), shows a maximum value of 59 K at 50% Hf and decreases with a deviation from the Hf composition. The decrease in ΔT_x is more distinct in the high Hf concentration range. The crystallization of the Cu–Hf alloys with a supercooled liquid region appears to occur through a single exothermic peak. The single exothermic peak of the 50% Hf alloy with the largest supercooled liquid has been confirmed to be due to the precipitation of the Cu_3Hf_z and Cu–Hf_z phases.

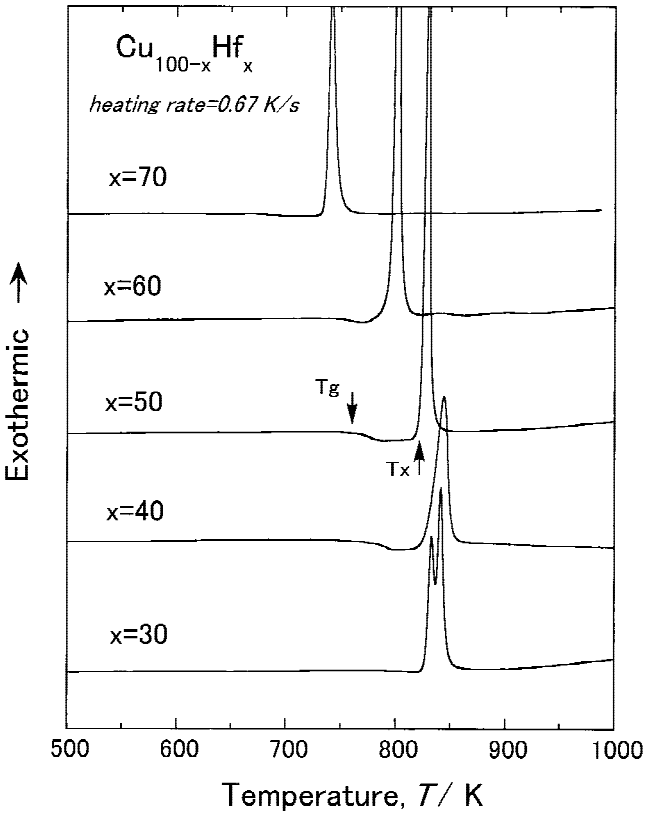

FIG. 1. DSC curves of melt-spun $Cu_{100-x}Hf_x$ (x = 30 to 70 at.%) glassy alloys.

Subsequently, we examined the effect of Ti addition on the glass transition and the thermal stability of supercooled liquid region in the alloy series of $Cu_{60}Hf_{40-x}Ti_x$. Figure 2 shows DSC curves of the melt-spun $Cu_{60}Hf_{40-x}Ti_x$ (x = 0 to 40 at.%) glassy alloys. In comparison with the $Cu_{60}Hf_{40}$ binary glassy alloy, the addition of 5% Ti leads to a significant increase in ΔT_x to 78 K through a decrease in T_g and an increase in T_x in the maintenance of the single-stage crystallization mode. However, with further increasing Ti content, the ΔT_x decreases due to the more significant decrease in T_x as compared with the decrease in T_g, accompanying the change in the crystallization mode from the single stage to multiple stages. The glass transition phenomenon disappears at 40% Ti. Figure 3 shows the changes in T_g, T_x, and ΔT_x as a function of Ti content for the melt-spun $Cu_{60}Hf_{40-x}Ti_x$ glassy alloys. One can confirm a monotonous decrease in T_g from 772 to 703 K over the whole Ti content, while T_x *shows a maximum* of 832 K at

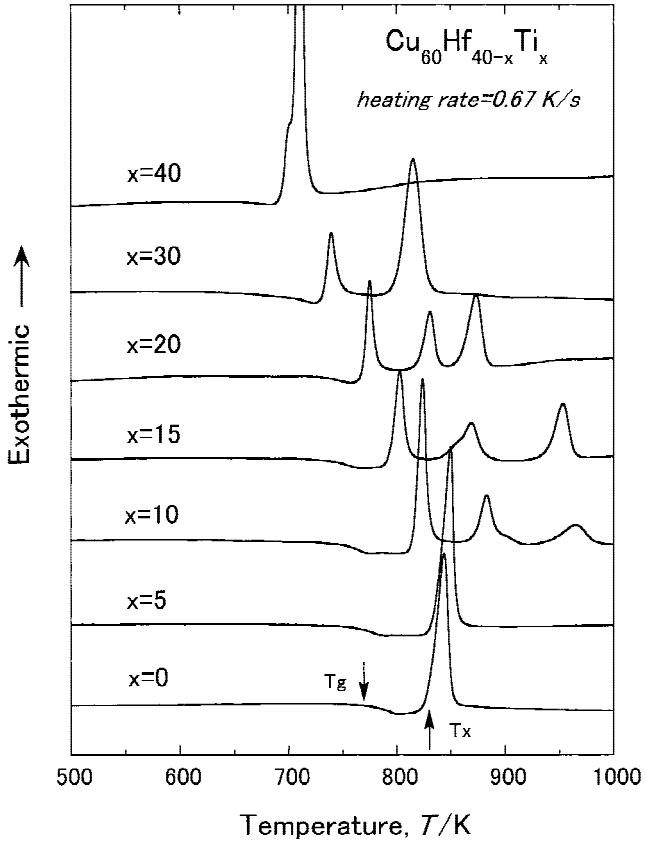

FIG. 2. DSC curves of melt-spun $Cu_{60}Hf_{40-x}Ti_x$ (x = 0 to 40 at.%) glassy alloys.

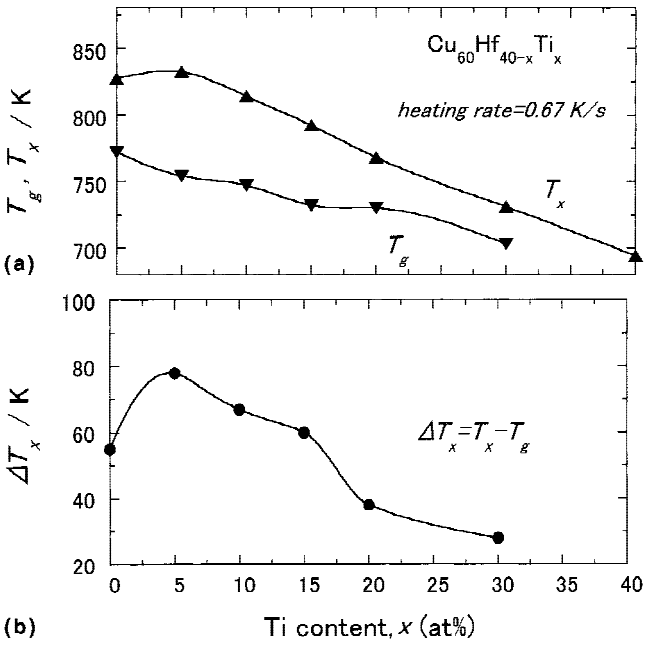

FIG. 3. Glass transition temperature (T_g), crystallization temperature (T_x), and supercooled liquid region ($\Delta T_x = T_x - T_g$) as a function of Ti content for melt-spun $Cu_{60}Hf_{40-x}Ti_x$ glassy alloys.

5% Ti and then decreases monotonously to 694 K at 40% Ti. As a result, ΔT_x shows a maximum of 78 K at 5% Ti, followed by a gradual decrease to 60 K at 15% Ti and then a significant decrease to 28 K at 30% Ti.

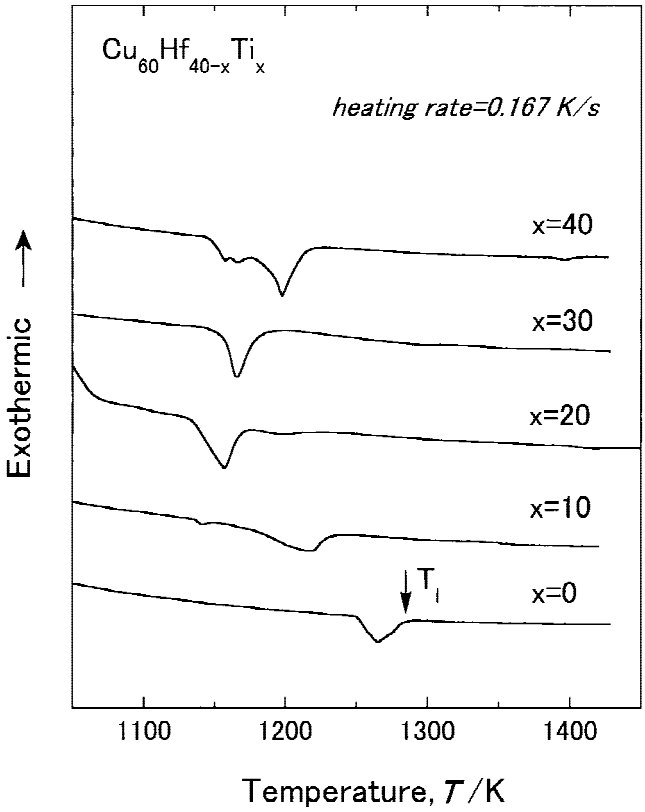

FIG. 4. DTA curves of the $Cu_{60}Hf_{40-x}Ti_x$ (x = 0 to 40 at.%) glassy alloys.

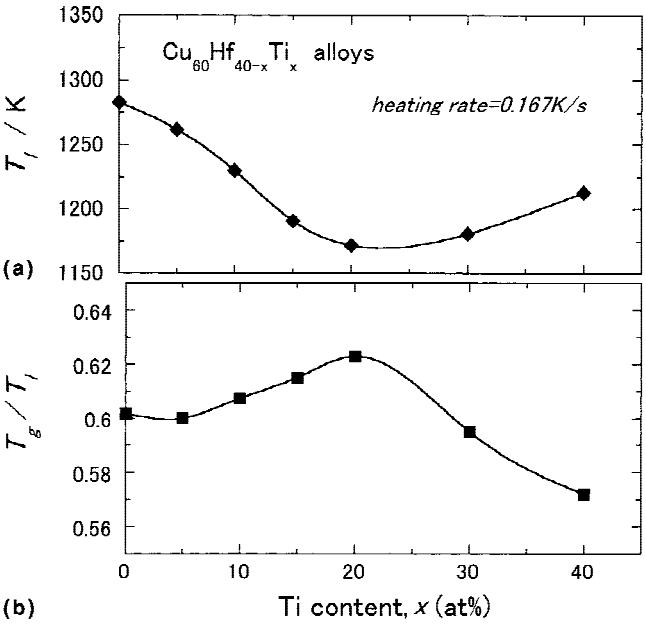

FIG. 5. Liquidus temperature (T_l) and reduced glass transition temperature (T_g/T_l) as a function of Ti content for the $Cu_{60}Hf_{40-x}Ti_x$ glassy alloys.

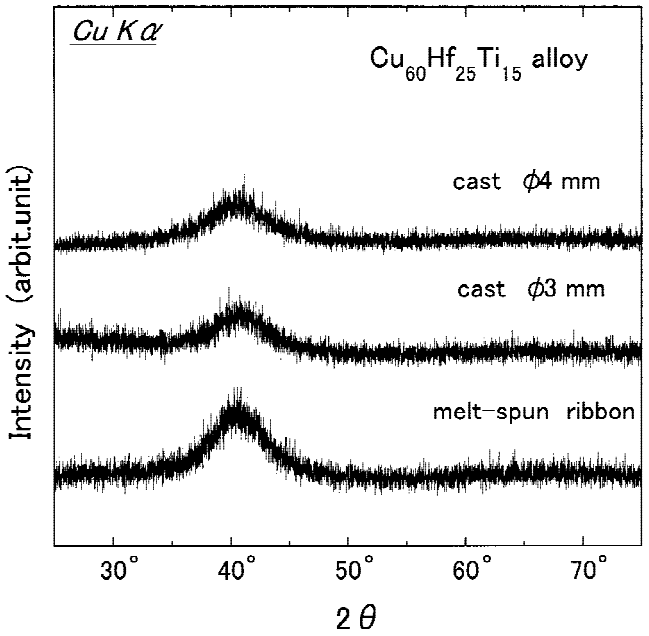

FIG. 6. XRD patterns of cast cylindrical $Cu_{60}Hf_{25}Ti_{15}$ rods with diameters of 3 and 4 mm. The data of the melt-spun ribbon are also shown for comparison.

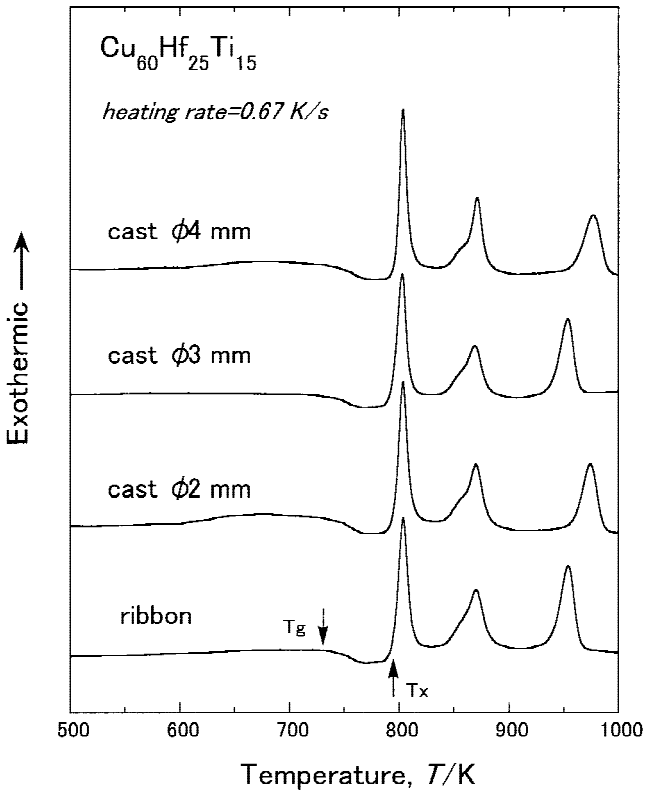

FIG. 7. DSC curves of cast $Cu_{60}Hf_{25}Ti_{15}$ glassy rods with different diameters of 2 to 4 mm. The data of the melt-spun ribbon are also shown for comparison.

It is expected that the decreases in T_g and T_x by the addition of Ti reflect the lowering in the liquidus temperature (T_l) of the $Cu_{60}Hf_{40-x}Ti_x$ alloys. Figure 4 shows DTA curves of the $Cu_{60}Hf_{40-x}Ti_x$ (x = 0 to 40 at.%) alloys. The endothermic peak due to melting is seen for all the alloys and the melting reaction appears to occur through a single stage for the $Cu_{60}Hf_{40}$, $Cu_{60}Hf_{20}Ti_{20}$, and $Cu_{60}Hf_{10}Ti_{30}$ alloys. On the basis of the data shown in Fig. 4, the T_l and the reduced glass transition temperature (T_g/T_l) were plotted as a function of Ti content for the $Cu_{60}Hf_{40-x}Ti_x$ alloys in Fig. 5. It is clearly seen that T_l shows a minimum of 1172 K at 20% Ti. As a result, the 20% Ti alloy exhibits a maximum T_g/T_l of 0.623. Here, it is noticed that the high T_g/T_l values exceeding 0.61 are obtained for the $Cu_{60}Hf_{30}Ti_{10}$, $Cu_{60}Hf_{25}Ti_{15}$, and $Cu_{60}Hf_{20}Ti_{20}$ glassy alloys. We have

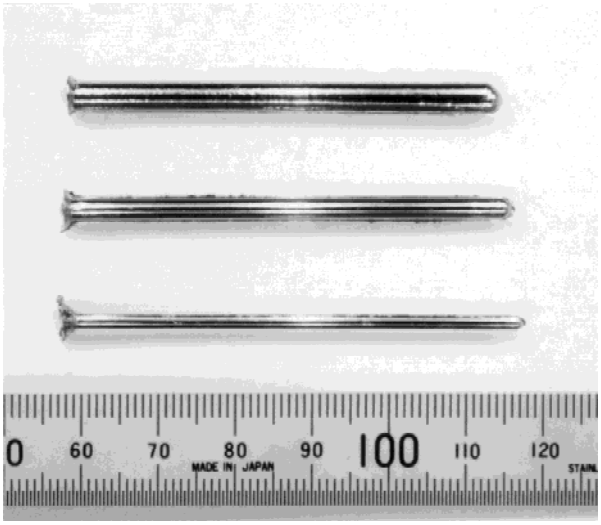

FIG. 8. Shape and outer surface appearance of cast $Cu_{60}Hf_{25}Ti_{15}$ glassy rods with diameters of 2, 3, and 4 mm.

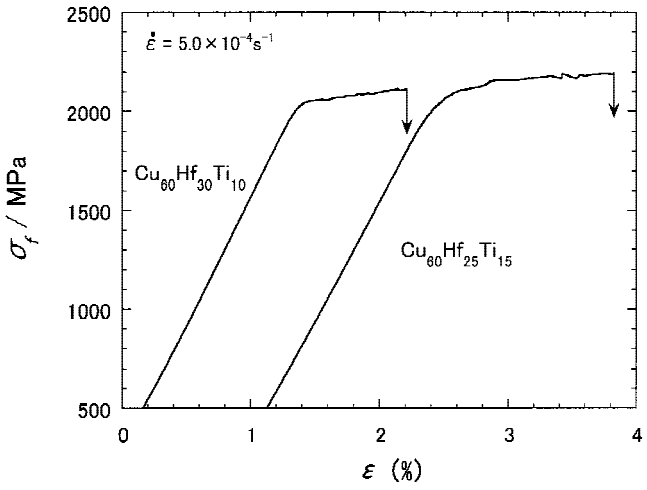

FIG. 9. Compressive stress-elongation curves of cast $Cu_{60}Hf_{30}Ti_{10}$ and $Cu_{60}Hf_{25}Ti_{15}$ glassy rods with a diameter of 2 mm.

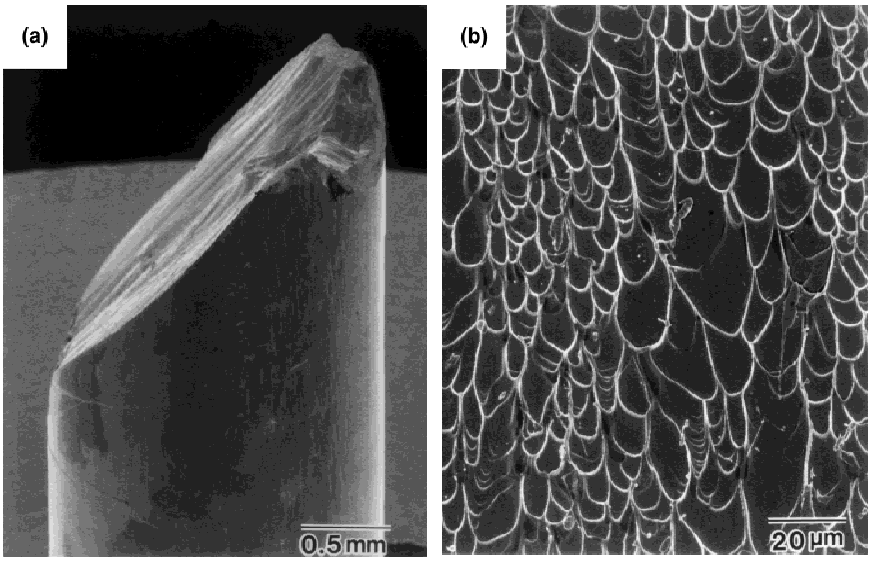

FIG. 10. Compressive fracture surface of the cast $Cu_{60}Hf_{25}Ti_{15}$ glassy rod.

also confirmed that the $Cu_{60}Zr_{40-x}Ti_x$ ($x = 0$, 10, and 20 at.%) glassy alloys show high T_g/T_1 exceeding 0.60 and the highest T_g/T_1 of 0.63 is obtained for the 20 at.% Ti alloy. Considering that a number of bulk glassy alloys are obtained for the alloys with high T_g/T_1 above 0.60 by the copper mold casting method,[22–24] it is expected that Cu-based bulk glassy alloys are formed by choosing the alloy compositions $Cu_{60}Hf_{40-x}Ti_x$ ($x = 10$ and 20%).

B. Formation of bulk glassy alloys

Figure 6 shows x-ray diffraction patterns of the cylindrical $Cu_{60}Hf_{25}Ti_{15}$ rods with diameters of 3 and 4 mm. No distinct crystalline peaks are seen for the 3- and 4-mm samples, indicating the formation of a single glassy phase in the diameter range up to 4 mm. Figure 7 shows DSC curves of the cast glassy alloy rods with diameters of 2, 3, and 4 mm, together with the data of the melt-spun glassy alloy ribbon. The T_g, T_x, and heat of crystallization are nearly the same among the bulk and ribbon samples, being consistent with the results obtained from XRD. As an example, the outer surface appearance of the cast bulk glassy rods with diameters of 2, 3, and 4 mm is shown in Fig. 8. These rod samples exhibit good metallic luster, and no appreciable concavity due to a crystalline phase is recognized. We have also confirmed the absence of a crystalline phase in the optical micrographs taken from the central region of the transverse cross section of the 2-, 3-, and 4-mm rod samples. Here, it is important to point out that the further increase in the sample diameter causes the formation of crystalline phases, and hence, the critical diameter of the ternary $Cu_{60}Hf_{25}Ti_{15}$ alloy lies between 4 and 5 mm.

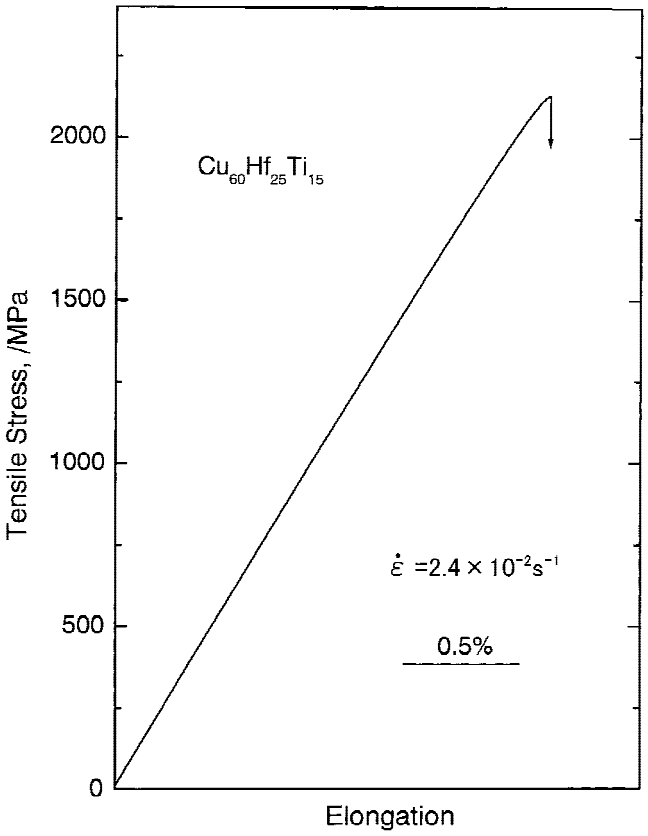

FIG. 11. Tensile stress-elongation curve of a cast $Cu_{60}Hf_{25}Ti_{15}$ glassy sheet with a gauge dimension of 1 mm in thickness, 2 mm in width, and 10 mm in length.

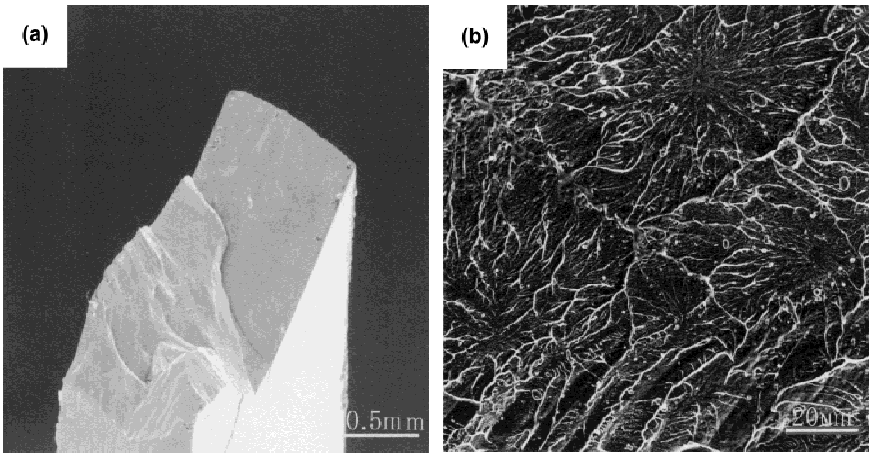

FIG. 12. Tensile fracture surface of the cast $Cu_{60}Hf_{25}Ti_{15}$ glassy sheet.

C. Mechanical properties of bulk glassy alloys

Figure 9 shows compressive stress–strain curves of the cast bulk glassy $Cu_{60}Hf_{30}Ti_{10}$ and $Cu_{60}Hf_{25}Ti_{15}$ rods. It is seen that the glassy rods exhibit elastic elongation in the elongation range up to 1.8%, followed by plastic elongation of about 0.8 to 1.6% and then final fracture, indicating that the new Cu-based bulk glassy alloys have rather good ductility. Young's modulus (E), compressive yield strength ($\sigma_{c,y}$), and compressive fracture strength ($\sigma_{c,f}$) are 119 GPa, 1995 MPa, and 2120 MPa, respectively, for the 30% Hf alloy and 124 GPa, 2010 MPa, and 2160 MPa, respectively, for the 25% Hf alloy. The fracture occurs along the maximum shear plane, which is declined by about 45° to the direction of applied load, and the fracture surface consists of a well-developed vein pattern typical to Zr-based bulk glassy alloys with good ductility,[22–24] as exemplified for $Cu_{60}Hf_{25}Ti_{15}$ in Fig. 10. It is noticed that the fracture strength exceeds 2000 MPa accompanying the distinct plastic elongations. The high fracture strength above 2000 MPa was also obtained in the tensile deformation mode. Figure 11 shows a tensile stress-elongation curve of the bulk glassy $Cu_{60}Hf_{25}Ti_{15}$ sheet. The E, tensile yield strength defined by the deviation point from the linear relation ($\sigma_{t,y}$), tensile fracture strength ($\sigma_{t,f}$), and fracture elongation including elastic elongation (ϵ_f) are 120 GPa, 1920 MPa, 2130 MPa, and 1.9%, respectively. The tensile fracture also occurs along the maximum shear plane and the developed vein pattern is seen over the whole fracture surface, as shown in Fig. 12. Furthermore, the Vickers hardness (H_v) was 670 for $Cu_{60}Hf_{25}Ti_{15}$ and 640 for $Cu_{60}Hf_{20}Ti_{20}$. Here, it is important to point out that the tensile fracture strength is nearly the same as the compressive fracture strength, indicating good ductility of the Cu-based bulk glassy alloy. There have been no data on high-strength Cu-based bulk alloys with high strength above 2000 MPa in crystalline and glassy states.[22–24,29] However, it is known that the perfect crystal Cu whisker of 1 μm in diameter exhibits high strength of 2000 MPa.[30] It is noticed that the tensile strength of the present bulk glassy alloy is comparable to that for the Cu whisker in spite of the much larger dimension of the specimen. In addition, the high strength level exceeding 2000 MPa has not been obtained for any Zr-based bulk glassy alloys in Zr–Al–Ni–Cu,[30,31] Zr–(Ti,Nb,Ta)–Al–Ni–Cu,[17,31–33] and Zr–Ti–Be–Ni–Cu[6] systems. Consequently, the present Cu-based bulk glassy alloys are expected to be developed as a new type of bulk structural material with higher strength combined with good ductility.

IV. DISCUSSION

As described above, the maximum sample thickness, ΔT_x, and T_g/T_l are 4 mm, 60 K, and 0.62 for the $Cu_{60}Hf_{25}Ti_{15}$ glassy alloy and 4 mm, 38 K, and 0.62 for the $Cu_{60}Hf_{20}Ti_{20}$ glassy alloy. In addition, ΔT_x and T_g/T_l of the $Cu_{60}Hf_{40}$ glassy alloy are 55 K and 0.60, respectively, and the critical sample diameter is about 1 mm. The relation among ΔT_x, T_g/T_l, and maximum sample thickness for the ternary and binary glassy alloys indicates that the glass-forming ability defined by the maximum sample thickness is related to ΔT_x and T_g/T_l. That is, the higher glass-forming ability for the new Cu-based alloys was obtained at the compositions with larger ΔT_x and higher T_g/T_l values. The increase in the ΔT_x implies that the thermal stability of supercooled liquid against crystallization increases by the addition of Ti. In addition, the increase in T_g/T_l results from the lowering of T_l. It is therefore concluded that the formation of the bulk glassy alloys results from the increase in the resistance of supercooled liquid against crystallization. It is also noticed in Fig. 3 that the crystallization of the supercooled liquid occurs through a single exothermic reaction accompanying the simultaneous precipitation of at least three crystalline phases. The crystallization mode

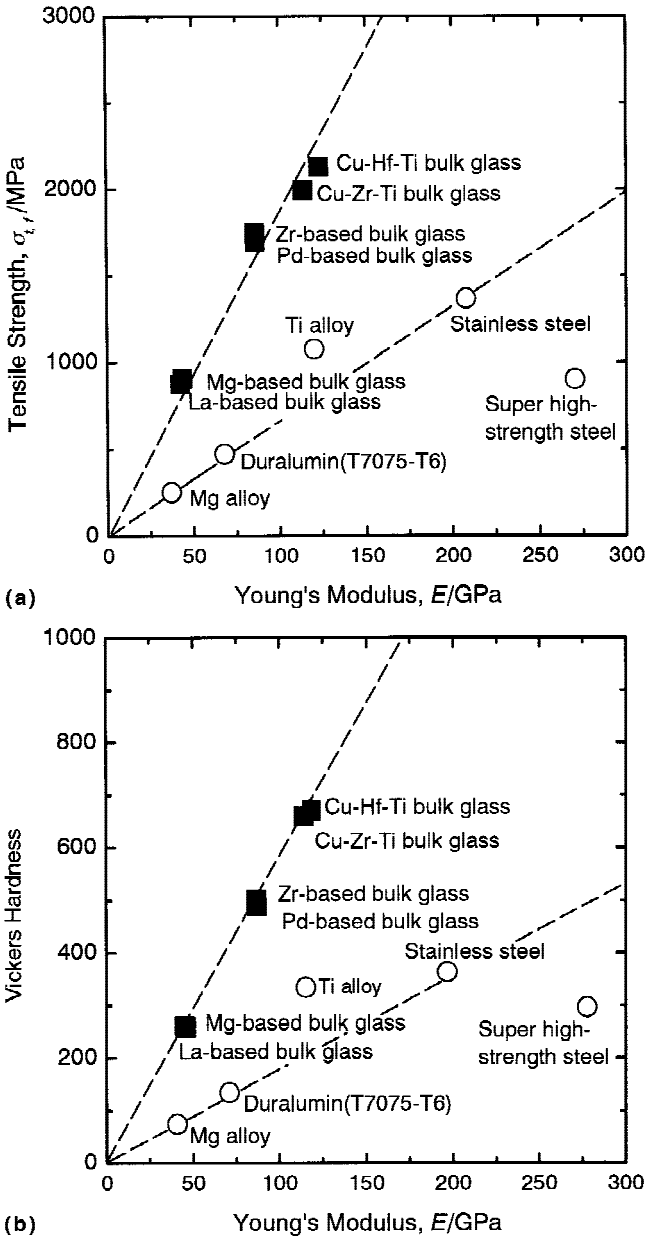

FIG. 13. Relationship between Young's modulus (E) and tensile fracture strength ($\sigma_{t,f}$) or Vickers hardness (H_v) for the cast $Cu_{60}Hf_{25}Ti_{15}$ glassy sheet. The data of other bulk glassy alloys and conventional crystalline alloys are also shown for comparison.

implies the necessity of long-range rearrangements of the constituent elements for the progress of crystallization. The necessity suppresses the crystallization reactions, resulting in the formation of bulk glassy alloys.

Next, we discuss the reason for the slight deviation from the direct correlation among glass-forming ability, ΔT_x and T_g/T_1. It has previously been reported that the high glass-forming ability leading to the formation of a bulk glassy alloy is obtained in the multicomponent alloy systems with the following three empirical rules:[22–24] (i) a multicomponent consisting of more than three

TABLE I. Glass transition temperature (T_g), crystallization temperature (T_x), supercooled liquid region ($\Delta T_x = T_x - T_g$), liquidus temperature (T_1), and reduced glass transition temperature (T_g/T_1) for Cu–Hf–Ti bulk glassy alloys. The data of the Cu–Zr–Ti and Zr–Al–Ni–Cu bulk glassy alloys are also shown for comparison.

Composition (at.%)	T_g (K)	T_x (K)	ΔT_x (K)	T_1 (K)	T_g/T_1
$Zr_{55}Al_{10}Ni_5Cu_{30}$	690	755	85	1113	0.62
$Zr_{60}Al_{10}Ni_{10}Cu_{20}$	676	770	94	1095	0.62
$Cu_{60}Zr_{30}Ti_{10}$	713	750	37	1153	0.62
$Cu_{60}Zr_{20}Ti_{20}$	708	768	38	1127	0.63
$Cu_{60}Hf_{25}Ti_{15}$	732	792	60	1191	0.62
$Cu_{60}Hf_{20}Ti_{20}$	730	768	38	1172	0.62

elements; (ii) significant atomic size mismatches above 12%; (iii) suitable negative heats of mixing. In the Cu–Hf–Ti system, their atomic sizes change in the order of Hf > Ti > Cu and the atomic size ratios are 1.08 for Hf/Ti and 1.14 for Ti/Cu.[34] In addition, the heats of mixing have been estimated to be −9 kJ/mol for Cu–Ti, −17 kJ/mol for Cu–Hf, and 0 kJ/mol for Hf–Ti.[35] These data on the atomic size ratios and heats of mixing imply that the present Cu-based alloys do not perfectly satisfy the three empirical rules. The insufficient condition is thought to result in a disagreement of alloy compositions where the largest ΔT_x and the highest T_g/T_1 are obtained. That is, the largest ΔT_x and the largest maximum sample thickness are obtained at 5% Ti and 10 to 15% Ti, respectively, while the highest T_g/T_1 is obtained at 20% Ti owing to the significant lowering of Ti at 20% Ti. The search for an appropriate element leading to agreement of the alloy compositions among the largest ΔT_x, the highest T_g/T_1, the lowest T_1, and maximum sample diameter is also expected to cause the formation of a bulk glassy alloy with a larger diameter.

It was shown in Fig. 11 that the Cu–Hf–Ti bulk glassy alloy exhibits high tensile fracture strength of 2130 MPa which is comparable to that (1700 to 2900 MPa) for a Cu whisker with perfect crystal structure[30] and much higher than that (1600 to 1700 MPa) for Zr-based bulk glassy alloys in Zr–Al–Ni–Cu,[31] Zr–(Ti,Nb)–Al–Ni–Cu,[17,31–33] and Zr–Ti–Be–Ni–Cu[6] systems. Here, we discuss the reason for the extremely high tensile fracture strength for the Cu-based bulk glassy alloy. Figure 13 summarizes the relationship between E and $\sigma_{t,f}$ or H_v for the $Cu_{60}Hf_{25}Ti_{15}$ bulk glassy alloy, together with the data of other bulk glassy alloys including the $Cu_{60}Zr_{30}Ti_{10}$ bulk glassy alloy.[21] There is a clear tendency for E to increase with an increase of $\sigma_{t,f}$ or H_v for all the bulk glassy alloys. The slope in the linear relation for the bulk glassy alloys is also significantly different from that for the conventional crystalline alloys. It is characterized that the bulk glassy alloys have lower Young's modulus, larger elastic elongation limit, and higher strength as compared with those for the conventional crystalline

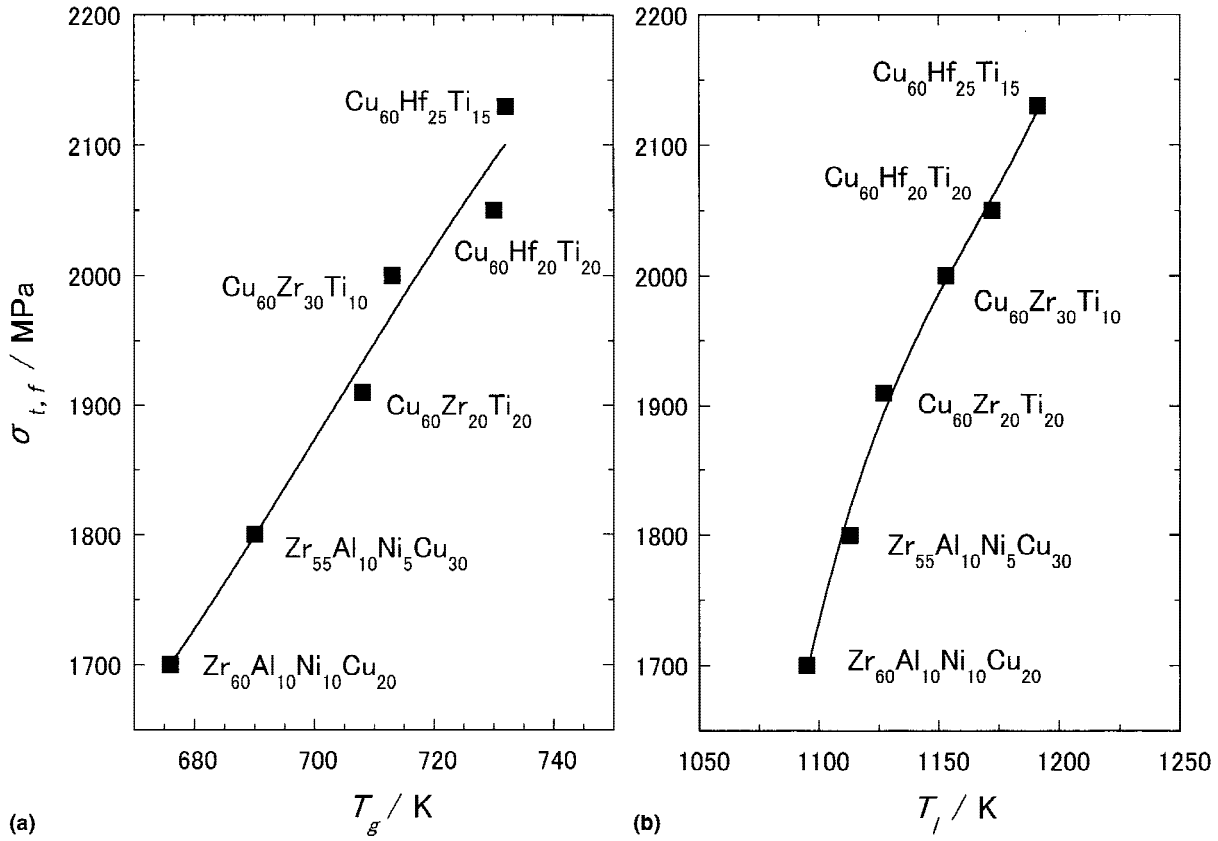

FIG. 14. Relationship between tensile fracture strength ($\sigma_{t,f}$) and glass transition temperature (T_g) or liquidus temperature (T_1) for the cast Cu–Hf–Ti glassy sheets. The data of the cast Cu–Zr–Ti and Zr–Al–Ni–Cu glassy alloys are also shown for comparison.

alloys. It has been pointed out that the T_g and T_1 of glassy alloys reflect the degree of bonding force among the constituent elements.[36] As shown in Table I, the T_g and T_1 of the Cu–Hf–Ti ternary glassy alloys are higher than those for the Zr–Al–Ni–Cu and Cu–Zr–Ti glassy alloys. The higher values of T_g and T_1 allow us to presume that the bonding force among the Cu, Hf, and Ti elements is stronger than that among the Zr, Al, Ni, and Cu elements as well as among the Cu, Zr, and Ti elements. In addition, the relations between $\sigma_{t,f}$ and T_g or T_1 for the Cu–Hf–Ti, Cu–Zr–Ti, and Zr–Al–Ni–Cu bulk glassy alloys are shown in Fig. 14. Although some scatterings are seen, one can recognize a strong correlation, demonstrating an appropriateness of the previous concept between strength and T_g or T_1.

V. SUMMARY

We have searched for a new Cu-based bulk glassy alloy with good mechanical properties which can be produced by the copper mold casting methods. The results obtained are summarized as follows.

(1) In the $Cu_{60}Hf_{40-x}Ti_x$ alloy system, T_g decreases monotonously with increasing Ti content, while T_x shows a maximum at 5 at.% Ti and T_1 shows a minimum at 20 at.% Ti. The resulting ΔT_x shows a maximum of 78 K at 5 at.% Ti, followed by a gradual decrease to 60 K at 15% Ti and then a significant decrease to 28 K at 30% Ti. No glass transition is observed for $Cu_{60}Ti_{40}$.

(2) The T_g/T_1 shows a maximum value of 0.62 at 20 at.% Ti because of the minimum value of 1172 K for T_l at 20%Ti.

(3) The bulk glassy alloys were formed in the ternary system, and the largest diameter is 4 mm for the $Cu_{60}Hf_{25}Ti_{15}$ alloy. The bulk glass-forming ability is more closely related to T_g/T_1 rather than ΔT_x.

(4) The bulk glassy alloys possess good mechanical properties, i.e., Young's modulus of 119 to 124 GPa, yield strength of 1995 to 2010 MPa, compressive fracture strength of 2120 to 2160 MPa, tensile fracture strength of 2130 MPa, elastic elongation of 1.6–2.0%, and compressive plastic elongation of 0.8 to 1.6%. The good combination of high glass-forming ability and good mechanical properties for the Cu-based alloys indicates the possibility of future development as a new type of bulk structural material.

REFERENCES

1. A. Inoue, T. Zhang, and T. Masumoto, Mater. Trans. JIM **30,** 965 (1989).

2. A. Inoue, K. Ohtera, K. Kita, and T. Masumoto, Jpn. J. Appl. Phys. **27,** L2248 (1988).
3. A. Inoue, T. Zhang, and T. Masumoto, Mater. Trans. JIM **31,** 425 (1990).
4. A. Inoue, A. Kato, T. Zhang, S.G. Kim, and T. Masumoto, Mater. Trans. JIM **32,** 609 (1991).
5. A. Inoue, T. Zhang, and T. Masumoto, Mater. Trans. JIM **31,** 177 (1990).
6. A. Peker and W.L. Johnson, Appl. Phys. Lett. **63,** 2342 (1993).
7. A. Inoue, T. Zhang, N. Nishiyama, K. Ohba, and T. Masumoto, Mater. Lett. **19,** 131 (1994).
8. A. Inoue and G.S. Gook, Mater. Trans. JIM **36,** 1180 (1995).
9. A. Inoue, N. Nishiyama, and T. Matsuda, Mater. Trans. JIM **37,** 181 (1996).
10. X.M. Wang and A. Inoue, Mater. Trans. JIM **41,** 542 (2000).
11. T. Itoi and A. Inoue, Mater. Trans. JIM **38,** 359 (1997).
12. A. Inoue, K. Ohtera, A.P. Tsai, and T. Masumoto, Jpn. J. Appl. Phys. **27,** L280 (1988).
13. Y. He, S.J. Poon, and G.J. Shiflet, Science **23,** 1640 (1988).
14. A. Inoue, M. Oguchi, K. Matsuzaki, and T. Masumoto, Int. J. Rapid Solidif. **1,** 273 (1984–5).
15. A. Inoue, N. Matsumoto, and T. Masumoto, Mater. Trans. JIM **31,** 493 (1990).
16. A. Inoue, N. Yana, and T. Masumoto, J. Mater. Sci. **19,** 3786 (1984).
17. A. Inoue, T. Shibata, and T. Zhang, Mater. Trans. JIM **36,** 1420 (1995).
18. X.H. Lin and W.L. Johnson, J. Appl. Phys. **78,** 6514 (1995).
19. T. Zhang and A. Inoue, Mater. Trans. JIM **40,** 301 (1999).
20. C. Li, J. Saida, M. Kiminami, and A. Inoue, J. Non-Cryst. Solids **261,** 108 (2000).
21. A. Inoue, W. Zhang, T. Zhang, and K. Kurosaka, Mater. Trans. **42,** 1149 (2001).
22. A. Inoue, Mater. Trans. JIM **36,** 866 (1995).
23. A. Inoue, Mater. Sci. Eng. A **226–228,** 357 (1997).
24. A. Inoue, Acta Mater. **48,** 279 (2000).
25. Metals Databook, edited by Japan Institute of Metals (Maruzen, Tokyo, Japan, 1983), p. 12.
26. A. Inoue and E. Makabe, Japanese Patent, 3011904 (1997).
27. H. Kakiuchi, A. Inoue, M. Onuki, Y. Takano, and T. Yamaguchi, Mater. Trans. JIM **42,** 678 (2001).
28. A. Inoue, C. Suryanarayana, and T. Masumoto, J. Mater. Sci. **16,** 1391 (1981).
29. Metals Handbook, edited by Japan Institute of Metals (Maruzen, Tokyo, Japan, 2000), p. 365.
30. Metals Handbook, edited by Japan Institute of Metals (Maruzen, Tokyo, 2000), p. 331.
31. T. Zhang and A. Inoue, Mater. Trans. JIM **39,** 1230 (1998).
32. T. Zhang and A. Inoue, Mater. Trans. JIM **39,** 859 (1998).
33. R.D. Conner, H. Choi Kim, and W.L. Johnson, J. Mater. Res. **14,** 3292 (1999).
34. Metals Databook, edited by Japan Institute of Metals (Maruzen, Tokyo, Japan, 1983), p. 8.
35. F.R. de Boer, R. Boom, W.C.M. Mattens, A.R. Miedema, and A.K. Niessen, *Cohesion in Metals* (North-Holland, Amsterdam, The Netherlands, 1988).
36. H.S. Chen, Rep. Prog. Phys. **43,** 353 (1980).